Journal of Magnetics 8(1), 18-23 (2003)

Microstructure and Magnetic Properties of Nanocomposite $Sm_2Fe_{15}Ga_2C_x/\alpha$-Fe Permanent Magnets

Zhao-hua Cheng*

State Key Lab. of Magnetism, Institute of Physics, Chinese Academy of Sciences, P.O. Box 603, Beijing 100080, China

(Received 10 December 2002)

In our previous work, microstructure and magnetic properties of two-phase exchange-coupled $Sm_2Fe_{15}Ga_2C_x/\alpha$-Fe nanocomposites have been investigated by means of x-ray diffraction, transmission electron microscopy and magnetization measurement. It was found the exchange coupling between the magnetically hard phase $Sm_2Fe_{15}Ga_2C_x$ and the magnetically soft one α-Fe results in an enhancement of the remanence. The sizes of crystallites of both phases are, however, much larger than the Bloch domain-wall width of the magnetically hard phase. This microstructure gives rise to a concave demagnetization curve and consequently reduces the maximum energy product. In order to improve their magnetic properties, a few percent of Zr, which may be effective to refine the microstructure through rapid quenching, was introduced into the nanocomposites. The addition of Zr was found to improve the magnetic properties significantly. Under optimum heat-treatment conditions, the remanence, coercivity and maximum energy product increase from 0.65 T, 0.48 T and 50 kJ/m^3 for the Zr-free sample to 0.72 T, 0.77 T and 71.6 kJ/m^3 for the 1 at.% Zr-containing one, respectively. The improvements of magnetic properties are due to the refinement of microstructure by the addition of Zr.

Key words : nanocomposites, microstructure, exchange coupling, refinement

1. Introduction

In the search for inexpensive iron-rich permanent magnets, the discovery of $Sm_2Fe_{17}(N,C)_x$ compounds prepared by gas-solid reaction method has attracted considerable research activities [1, 2]. $Sm_2Fe_{17}(N,C)_x$ compounds seem to be very promising candidates as permanent magnets. Unfortunately, the poor thermal stability restricts their practical application as sintered magnets. In order to improve the thermal stability, Shen and coworkers have investigated the effect of Ga, Al or Si substitution for Fe in $Sm_2Fe_{17}C_x$ on the structure and magnetic properties [3-5]. It was found that a small amount of Ga, Al or Si could not only stabilize the 2:17-type structure with high carbon concentration, but also increase significantly the uniaxial anisotropy field as well as the Curie temperature. The arc-melted carbides with these additives are quite stable, retaining the 2:17 structure even at temperature above 1000 °C, and have high Curie temperature ($\approx$ 630 K) as well as strong uniaxial anisotropy (> 12 T at room temperature). These advantages make them suitable for the raw materials of sintered permanent magnets. Room-temperature coercivities of 1.2~1.6 T have been achieved directly by melt-spinning technique in samples with a nearly single-phase $Sm_2Fe_{15}Ga_xC_{2.5}$ structure (x = 2 and 3) [6]. High coercivities of 1.2~1.5 T at room temperature have been also obtained in melt-spun and mechanically-alloyed Sm-Fe-Ga-C compounds by a subsequent heat-treatment [7, 8]. A significant increase in coercivity up to 2.2 T at room temperature has been found in melt-spun Sm-Fe-Ga-C with an excess of Sm [9]. However, the introduction of non-magnetic Ga atoms decreases the saturation magnetization monotonically and the maximum energy product of single-phase $Sm_2Fe_{15}Ga_2C_2$ is only 45 kJ/m^3. In order to obtain a high value of maximum energy product, it is necessary to improve remanence and to keep the coercivity sufficiently high. Recently, a significant enhancement of remanence has been observed in two-phase exchange-coupled nanocomposites [10-13]. Based on the theory of micromagnetism, some work has been performed to explain the mechanism of remanence enhancement and to simulate the magnetization reversal process [14, 15]. The nanocomposite permanent magnets with optimum microstructure are expected to have an energy product up to 1 MJ/m^3 and can be used as

*Corresponding author: Tel: +86-10-82649282, e-mail: zhcheng@g203.iphy.ac.cn

inexpensively bonded magnets due to the low rare earth concentration [16]. Most of the early work in this field was focused on the systems of $Nd_2Fe_{14}B$/a-Fe and $Sm_2Fe_{17}N_x/\alpha$-Fe [10-13, 15, 16], the investigations of magnetic properties of nanocomposite Sm-Fe-Ga-C with an excess of α-Fe are relatively few [7, 17]. Recently, we have successfully synthesized nanocomposites composed of $Sm_2Fe_{15}Ga_2C_x$ and α-Fe by direct melt-spinning and investigated the relationship between their microstructure and magnetic properties [18]. Since the grain sizes of both magnetically hard and soft phases are much larger than the domain-wall width of magnetically hard phase, the demagnetization curve shows a concave shape and consequently gives rise to a relatively low maximum energy product. In order to refine the microstructure and to improve the magnetic properties, a few percent of additive Zr was introduced into the $Sm_2Fe_{15}Ga_2C_x/\alpha$-Fe nanocomposites. In this paper, the influence of Zr on their microstructures and magnetic properties was investigated.

2. Experimental

The alloys with nominal composition of $Sm_8Fe_{72}Ga_8C_{12}$ (A), $Sm_{7.9}Fe_{71.3}Ga_{7.9}Zr_1C_{11.9}$ (B) and $Sm_{7.8}Fe_{70.6}Ga_{7.8}Zr_2C_{11.8}$ (C) were prepared by arc-melting. Iron and carbon were first melted together in an induction furnace to form Fe-C prealloy with lower melting temperature. Then Sm, Ga, Fe and Fe-C prealloy were arc-melted together in a highly pure argon atmosphere. The elements used were at least 99.9% in purity. An excess of 5 at.% Sm was added to compensate the evaporation loss during melting. The ingot alloys were re-melted at least six times to achieve good homogeneity. The as-quenched ribbons with a width of about 2.5 mm and a thickness of about 25 μm were prepared by melt-spinning in a highly pure helium atmosphere at the surface velocity $v_s = 35$ m/s. Both x-ray diffraction (XRD) patterns and thermomagnetic curves confirm the amorphous state of the as-quenched ribbons. The heat-treatments were performed at the temperature range of 700~900 °C for 15 minutes in high vacuum, and then quench the samples to room temperature. The phase composition of crystallized alloys was checked by means of XRD patterns with Cu Kα radiation and thermomagnetic curves. The chemical analysis showed that the carbon content was about 9.3 at.%, which corresponds to $x \approx 2.2$ in the $Sm_2Fe_{15}Ga_2C_x$ phase. In order to minimize the demagnetization effect, the magnetization measurement was performed using a vibrating sample magnetometer (VSM) with a maximum field of 7 T along the ribbon planes. The microstructural properties, such as, the size of crystallites and their distributions were investigated by using transmission electron microscopy (TEM).

3. Results and Discussion

3.1. Phase composition

The as-quenched ribbons were found to be amorphous, while the crystallized Zr-containing samples were composed of $Sm_2Fe_{15}Ga_2C_x$ with the Th_2Zn_{17}-type (2:17) structure and α-Fe. In addition to these two phases, a small amount of impurity phase existed in the Zr-free samples. For example, Figure 1 illustrates the XRD patterns of 1 at.% Zr-containing samples annealed at various temperatures. For the sample annealed at 700 °C, the XRD pattern shows very broad peaks, implying the grain sizes of both $Sm_2Fe_{15}Ga_2C_x$ and α-Fe are too fine to be resolved by XRD or the attribution of $TbCu_7$-type disorder structure. When the samples are annealed above 750 °C for 15 minutes, XRD patterns show well-resolved peaks. No obviously preferential orientation of the crystallites is observed from the diffraction peaks. Therefore, it may be inferred that the structure is crystallographically isotropic. The peaks of both 2:17 phase and α-Fe become much sharper with increasing the annealing temperatures, implying the grain sizes grow rapidly at high annealing temperatures.

The phase composition obtained from the thermomagnetic curves, as shown in Figure 2, is in good agreement

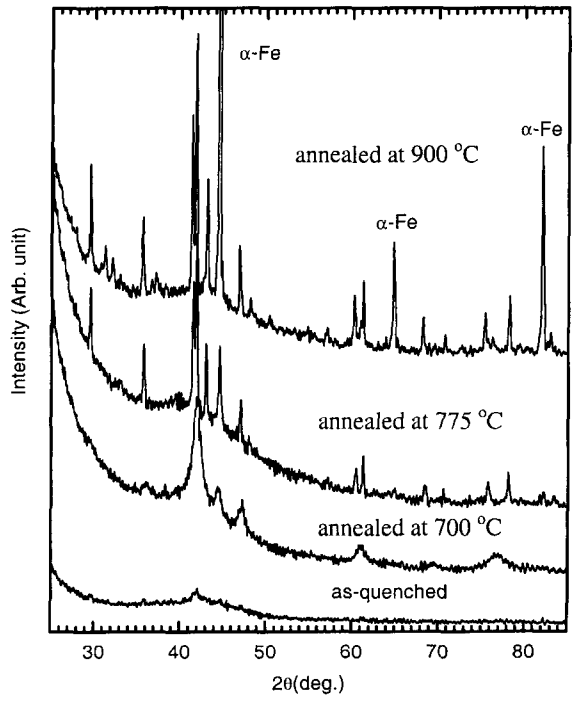

Fig. 1. XRD patterns of 1 at.% Zr-containing samples annealed at various temperatures.

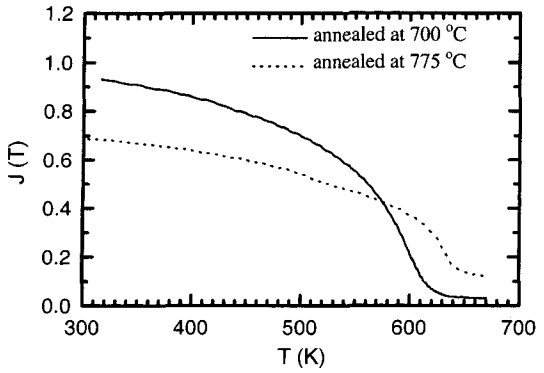

Fig. 2. Thermomagnetic curves of 1 at.% Zr-containing samples annealed at various temperatures in the field of 0.1 T.

with the XRD results. For the crystallized Zr-containing samples, there is one magnetic phase transition in the temperature range of 300~700 K. The magnetic phase transition observed at the temperature around 630 K, being close to that of $Sm_2Fe_{15}Ga_2C_{2.5}$ [6], corresponds to the Curie temperature of the 2:17-type phase. For the sample annealed at 700 °C, the magnetic phase transition temperature is slightly lower than that of the sample annealed at 775 °C. The slight difference in Curie temperature may be due to the formation of $TbCu_7$-type disorder structure during the initial crystallization process. The magnetic phase transition of α-Fe, because of its high Curie temperature (1043 K), is not observed in this temperature range.

3.2. Effect of annealing temperature on the hard magnetic properties

The as-quenched ribbons possess very low coercivity due to the lack of atomic long-range order in amorphous alloys. When they were annealed at the temperatures above 700 °C, the coercivity increases initially with increasing annealing temperature, gets relatively high values over a broad temperature range of 750~850 °C, then decreases with further increasing annealing temperature. Table 1 summarizes the effect of annealing temperature on the intrinsic coercivity, remanence and maximum energy product. The samples annealed at 700 °C show low coercivity and high remanence. The coercivity increases with increasing annealing temperature, but at the expense of the remanence. The energy product shows a small increase at low annealing temperature and decreases with further increasing annealing temperature. Under the optimum heat-treatment condition, the remanence, intrinsic coercivity and maximum energy product increase from 0.65 T, 0.48 T and 50 kJ/m^3 for the Zr-free sample to 0.72 T, 0.77 T and 71.6 kJ/m^3 for the sample containing 1 at.% Zr, respectively. In comparison with the single-phase $Sm_2Fe_{15}Ga_2C_2$ nanocrystalline alloy, the maximum energy product of the Zr-containing sample enhances about 60% [6].

Table 1. Effect of annealing temperature (T_a) on the magnetic properties of nanocomposite $Sm_2Fe_{15}Ga_2C_2/\alpha$-Fe permanent magnets

Samples	T_a (°C)	J_r (T)	$\mu_0 H_c$ (T)	$(BH)_{max}$ (kJ/m^3)
A	700	0.71	0.30	46.2
	750	0.65	0.48	50.0
	775	0.63	0.49	46.2
	800	0.64	0.55	44.6
	850	0.64	0.56	41.4
	900	0.72	0.09	7.2
B	700	0.89	0.27	70.8
	750	0.71	0.77	70.8
	775	0.72	0.77	71.6
	800	0.71	0.75	61.3
	850	0.73	0.28	20.0
	900	0.69	0.18	10.3
C	700	0.89	0.25	62.9
	750	0.65	0.64	54.9
	775	0.64	0.68	53.3
	800	0.64	0.65	46.2
	850	0.67	0.35	21.5
	900	0.72	0.21	13.5

3.3. The relationship between microstructure and hard magnetic properties

Figure 3 presents the TEM micrographs of the Zr-free and Zr-containing samples annealed at 700 °C, respectively. TEM observation indicates that the major phase $Sm_2Fe_{15}Ga_2C_x$ has larger crystallites, while the minor phase has smaller crystallites and locates as isolated particles at the grain boundaries between the major phase. The grain sizes in the Zr-containing sample are much smaller that those in the Zr-free one. Furthermore, it can be seen that the grain growth in the Zr-containing sample is not yet perfect.

Figure 4 presents the TEM micrographs of the Zr-free and Zr-containing samples annealed at 800 °C and 775°C for 15 minutes, respectively. The grain sizes are found to increase rapidly with increasing annealing temperature. The grain sizes of both 2:17 phase and α-Fe in the Zr-free sample show very broad distributions from 50~140 nm and 20~50 nm, respectively. The additive Zr appears to be very effective to retard the grain growth during the crystallization even at high annealing temperatures. The grain sizes of these two phases are finer and their distributions become narrower with introducing Zr and distribute in the range of 40~70 nm and 13~30 nm,

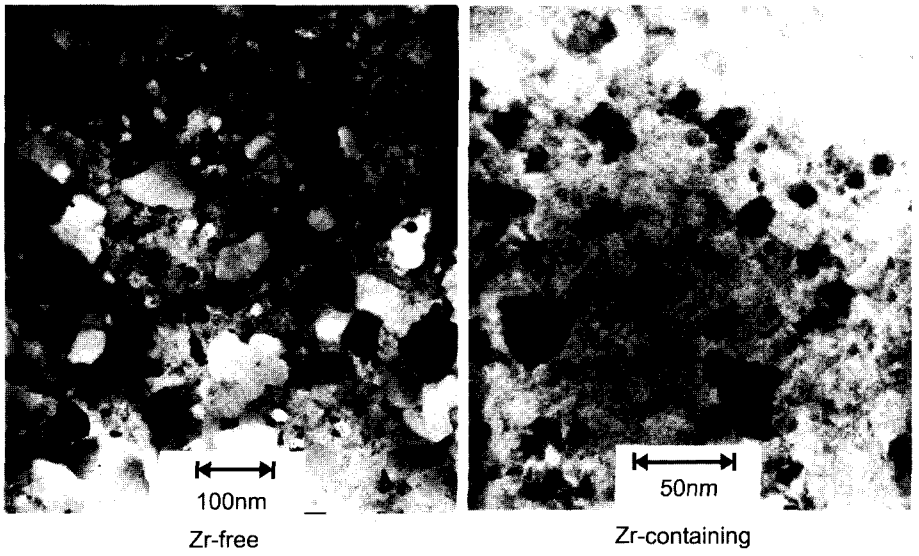

Fig. 3. TEM micrographs of the Zr-free and Zr-containing samples annealed at 700 °C.

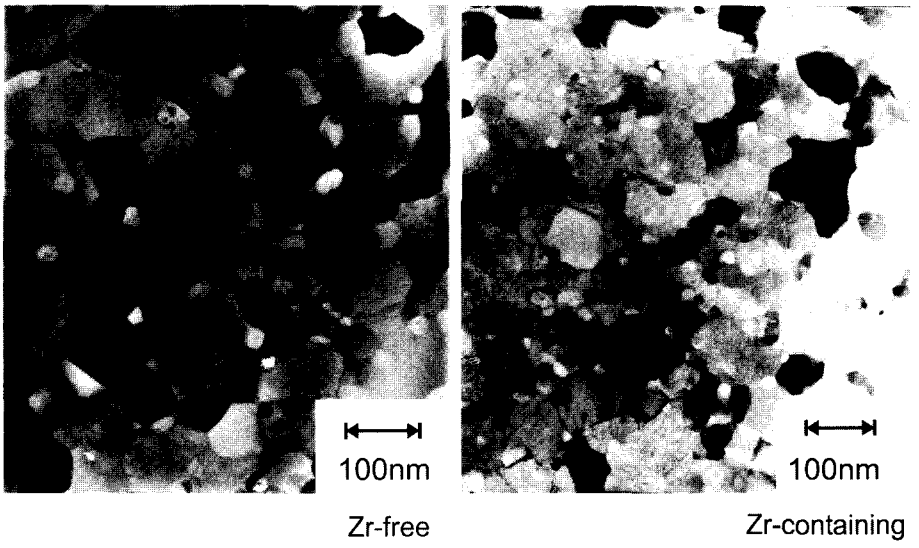

Fig. 4. TEM micrographs of the Zr-free and Zr-containing samples annealed at 800 and 775 °C, respectively.

respectively.

Figures 5(a) and 5(b) illustrate the room-temperature hysteresis loops of the Zr-free and 1 at.% Zr-containing samples annealed at different temperatures. Although there are two different magnetic phases in these crystallized samples, the hysteresis loops for the samples annealed at the temperatures between 700~800 °C show a nearly single-phase hard magnetic behavior. Owing to the refined microstructure of the Zr-containing samples, their hysteresis loops are more rectangular than those of the Zr-free samples. The reduced remanence ratios are found to be as high as 0.6~0.8. The values are obviously higher than the theoretical limit of the isotropic grains without exchange coupling. The remanence enhancement and the smooth demagnetization curves in two-phase composites are due to the exchange coupling between the magnetically hard $Sm_2Fe_{15}Ga_2C_x$ and the magnetically soft α-Fe. An enhancement of the remanence was reported in melt-spun Nd-Fe-B nanocrystalline homogeneous grains without any non-magnetic phases to separate adjacent grains [19]. In two-phase permanent magnets the remanence enhancement owing to exchange interactions is much more significant because most of magnetic moments of the magnetically soft phase are aligned to the average direction of the easy axes of the neighboring hard magnetic grains. The α-Fe particles in the neighborhood of the hard magnetic grains $Sm_2Fe_{15}Ga_2C_x$ are exchange-hardened. However, the exchange-coupling between magnetically hard and

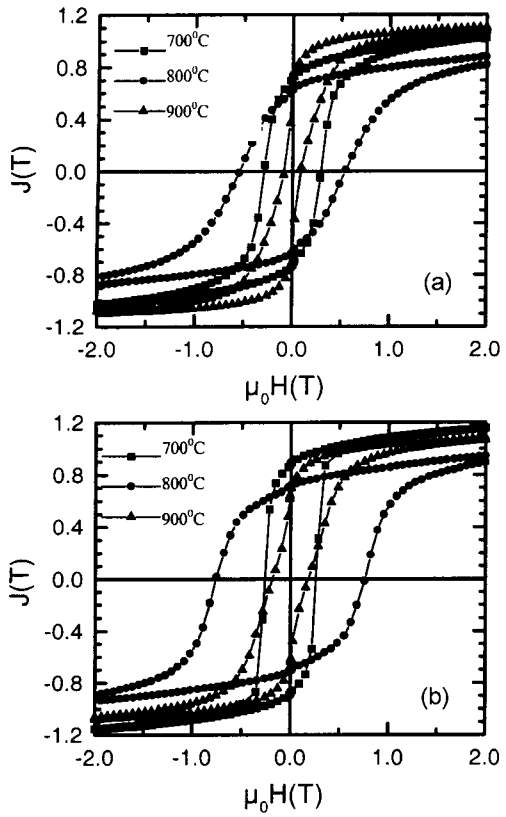

Fig. 5. Room-temperature hysteresis loops of the Zr-free (a) and 1 at.% Zr-containing samples (b) annealed at different temperatures.

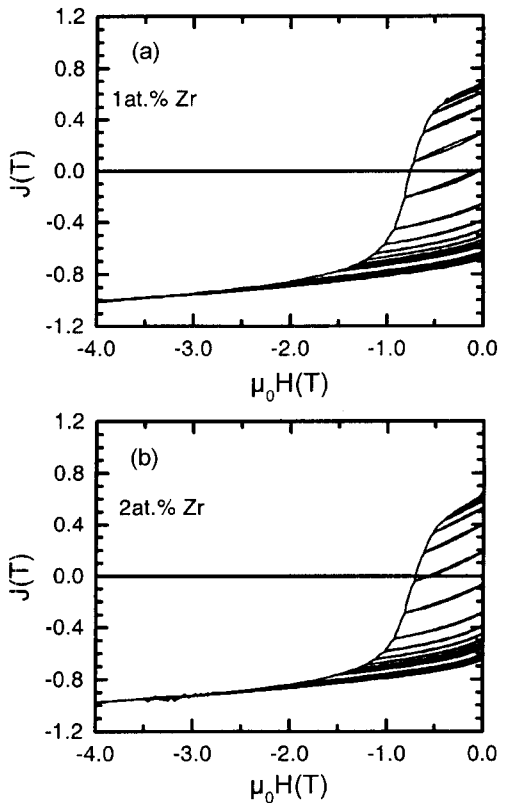

Fig. 6. DCD curves for the Zr-containing samples annealed at 775 °C.

soft phases becomes less effective to prevent the magnetization reversal of α-Fe if the mean grain sizes are much larger than the domain-wall width of the magnetically hard phase. TEM micrographs show that the grain sizes in the samples annealed at 900 °C are larger than 150 nm, much larger than the domain-wall width of $Sm_2Fe_{15}Ga_2C_x$ (4 nm). Thus, the magnetic moments of α-Fe reverse separately and the demagnetization curves are constricted for the samples annealed above 850 °C.

3.4. "Exchange-spring" behavior in nanocomposites

One of the characteristics for the nanocomposites is the presence of the "exchange-spring" mechanism [14, 20]. The "exchange-spring" behavior originates from the reversible rotation of the magnetically soft component for fields not large enough to reverse the magnetically hard one. In order to investigate the "exchange-spring" behavior, it is useful to measure dc demagnetization remanence curve (DCD). Fig. 6 illustrates room-temperature DCD curves for the Zr-containing sample annealed at 775 °C for 15 minutes. It can be seen from Fig. 6 that the recoil curves show a comparatively high degree of reversibility in the fields below coercivity. In order to determine the nucleation field H_n for reversing the magnetically hard phase, it is useful to investigate the irreversible and reversible portions in the DC demagnetization curve. Fig. 7(a) and (b) show the irreversible portion $\Delta J_{irr}=(J_r-J_d(H))/2J_r$ and the reversible portion ΔJ_{rev} versus H, where J_d(H) and J_r are the dc field demagnetization remanence in DCD curve and remanence after saturation, respectively. The $\Delta J_{irr}(H)$ curves can be explained according to one-dimension purely inhomogenous magnetization rotation model. The nucleation field of about 0.65 T has been obtained by the best fit of a corresponding plot of sinq versus $\mu_0 H_n/\cos\theta$ to the experimental curves $\Delta J_{irr}(H)$ [14]. The ΔJ_{rev} curve shows a peak at the nucleation field. At the critical field, the values of ΔJ_{irr} are 0.3 and 0.1 for the samples of Zr-free and Zr-containing samples, which implies about 30% of the moments have rotated irreversibly in Zr-free sample, while the irreversible portion is only 10% for the 1 at.% Zr-containing sample. These results suggest that a few percent of Zr addition can optimize the microstructure of $Sm_2Fe_{15}Ga_2C_x/\alpha$-Fe nanocomposites [14]. With decreasing the mean grain size, the exchange coupling becomes more dominant and will be more effective to align the moments of α-Fe parallel to the average direction of the easy axes of the neighboring

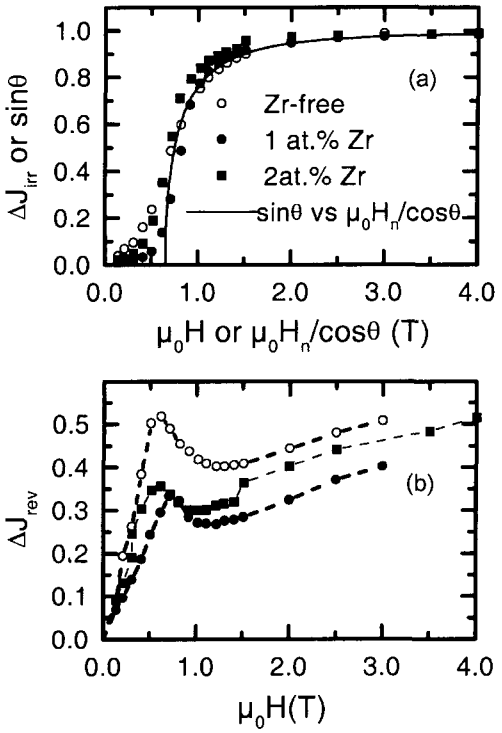

Fig. 7. The irreversible portion $\Delta J_{irr}=(J_r-J_d(H))/2J_r$ (a) and the reversible portion ΔJ_{rev} (b) versus H.

magnetically hard $Sm_2Fe_{15}Ga_2C_x$ grains and prevent the magnetization reversal of α-Fe. Thus, both remanence and coercivity increase with decreasing the mean grain size of nanocomposites. The significant improvements of magnetic properties are related to the refinement of microstructure by introducing additive Zr.

4. Conclusion

(1) The nanocomposite $Sm_2Fe_{15}Ga_2C_x/\alpha$-Fe permanent magnets have been successfully synthesized by means of the melt-spinning technique and the relationship between their microstructure and magnetic properties have been investigated.

(2) It is found that Zr is very effective additive in refining the microstructure. The Zr-containing samples show small grain sizes with relatively homogenous distribution.

(3) A few percent of Zr addition can increase both remanence and coercivity. Furthermore, the demagnetization curve shape is optimized by the introduction of Zr. Therefore, the maximum energy product of the Zr-containing sample is significantly higher than that of the Zr-free sample. The improvements of hard magnetic properties are related to the contribution of the microstructure refinement.

Acknowledgments

This work was supported by the State Key Project of Fundamental Research, the National Natural Sciences Foundation of China. Z.H. Cheng thanks the Alexander von Humboldt Foundation for financial support.

References

[1] J. M. D. Coey and H. Sun, J. Magn. Magn. Mater. **87**, L251 (1990).
[2] X. P. Zhong, R. J. Radwanski, F. R. de Boer, T. H. Jacobs, and K. H. J. Buschow, J. Magn. Magn. Mater. **86**, 333 (1990).
[3] B. G. Shen, L. S. Kong, F. W. Wang, and L. Cao, Appl. Phys. Lett. **63**, 2288 (1993).
[4] Z. H. Cheng, B. G. Shen, F. W. Wang, J. X. Zhang, H. Y. Gong, and J. G. Zhao, J. Phys.: Condens. Matter. **6**, L185 (1994).
[5] B. G. Shen, B. Liang, F. W. Wang, Z. H. Cheng, H. Y. Gong, S. Y. Zhang, and J. X. Zhang, J. Appl. Phys. **77**, 2637 (1995).
[6] B. G. Shen, L. S. Kong, H. Y. Gong, Z. H. Cheng, B. Liang, and F. W. Wang, J. Alloys & Compounds. **227**, 82 (1995).
[7] G. C. Hadjipanayis, Y. H. Zheng, A. S. Murthy, W. Gong, and F. M. Yang, J. Alloys & Compounds **222**, 49 (1995).
[8] L. Cao, K. H. Müller, A. Handstein, W. Grünberger, V. Neu, and L. Schultz, J. Phys.: D: Appl. Phys. **29**, 271 (1996).
[9] J. van Lier, M. Seeger, and H. Kronmüller, J. Magn. Magn. Mater **167**, 43 (1997).
[10] R. Coehoorn, D. B. de Mooij, J. P. W. B. Duchateau, and K. H. J. Buschow, J. Phys. (France) Colloq. **49**, C8-669 (1988).
[11] B. G. Shen, L. Y. Yang, J. X. Zhang, B. X. Gu, T. S. Ning, F. Wo, J. G. Zhao, H. Q. Guo, and W. S. Zhan, Solid State Commun. **74**, 839 (1990).
[12] A.Manaf, R. A. Buckley, and H. A. Davies, J. Magn. Magn. Mater **128**, 302 (1993).
[13] J. Ding, P. G. McCormick, and R. Street, J. Magn. Magn. Mater **124**, L1 (1993).
[14] E. F. Kneller and R. Hawig, IEEE Trans. Magn. **27**, 3588 (1991).
[15] T. Schrefl, J. Fidler, and H. Kronmüller, Phys. Rev. B **49**, 6100 (1994).
[16] R. Skomski and J. M. D. Coey, Phys. Rev. B. **48**, 15812 (1993).
[17] E. H. Feutrill, P. G. McCormick, and R. Street, J. Phys. D: Appl. Phys. **29**, 2320 (1996).
[18] Z. H. Cheng, J. X. Zhang, H. Q. Guo, J. van Lier, H. Kronmüller, and B. G. Shen, Appl. Phys. Lett. **72**, 1110 (1998).
[19] R. W. McCallum, A. M. Kadin, G. B. Clemente, and J. E. Keem, J. Appl. Phys. **61**, 3577 (1987).
[20] I. Panagiotopoulos, L. Withanawasam, and G. C. Hadjipanayis, J. Magn. Magn. Mater. **152**, 353 (1996).